The paper is published as:
Allahvirdi-Zadeh A, Wang K, El-Mowafy A (2021) POD of small LEO satellites based on precise real-time MADOCA and SBAS-aided PPP corrections. GPS Solutions, 25, 31. doi: 10.1007/s10291-020-01078-8. url: https://link.springer.com/article/10.1007%2Fs10291-020-01078-8

POD of small LEO satellites based on precise real-time MADOCA and SBAS-aided PPP corrections

Amir Allahvirdi-Zadeh[1], Kan Wang[1,*], Ahmed El-Mowafy[1]

[1] School of Earth and Planetary Sciences, Curtin University, Perth, Australia;

Amir.Allahvirdizadeh@curtin.edu.au; A.El-Mowafy@curtin.edu.au;

*Correspondence: kan.wang@curtin.edu.au

Abstract For real-time precise orbit determination (POD) of low earth orbit (LEO) satellites, high-accuracy global navigation satellite system (GNSS) orbit and clock products are necessary in real-time. Recently, the Japanese multi-GNSS advanced demonstration of orbit and clock analysis (MADOCA) precise point positioning (PPP) service and the new generation of the Australian/New-Zealand satellite-based augmentation system (SBAS) aided PPP service, provide free and precise GNSS products that are directly broadcast through the navigation and geostationary earth orbit (GEO) satellites, respectively. With the high quality of both products shown in this study, a 3D accuracy of centimeters can be achieved in the post-processing mode for the reduced-dynamic orbits of small LEO satellites having a duty cycle down to 40%, and at sub-dm to dm-level for the kinematic orbits. The results show a promising future for high-accuracy real-time POD onboard LEO satellites benefiting from the precise free-of-charge PPP corrections broadcast by navigation systems or SBAS.

Keywords: MADOCA; SBAS; LEO; POD; PPP

Introduction

The precise orbit determination (POD) of the low earth orbiters (LEO) has been investigated for decades. With the help of Global Navigation Satellite System (GNSS) observations collected onboard, high POD accuracy can be achieved using both the reduced-dynamic method (Wu et al. 1991) and the kinematic method (Švehla and Rothacher 2003). The former approach delivers typically higher accuracy, i.e., at centimeters, combining comprehensive dynamic models with the GNSS measurements, while the latter is

based on the kinematic precise point positioning (PPP) method based on purely GNSS measurements. In both POD approaches, when using undifferenced observations, precise GNSS satellite clocks and orbits are required, which can be obtained with some latencies, e.g., using the final or rapid products from the International GNSS Service (IGS) (Johnston et al. 2017). Similar corrections can be obtained from other analysis centers such as the Center for Orbit Determination in Europe (CODE), or in real-time, e.g., using the IGS real-time service (RTS) (Hadas and Bosy 2015). The (near)-real-time POD is essential for applications like atmospheric sounding or urgent Interferometric Synthetic Aperture Radar (InSAR). As examples for the near-real-time POD, the Metop-A satellite has achieved cm orbital accuracy by using the Real-Time Clock Estimation system (RETICLE) products from the German Aerospace Center (DLR) with less than 10 s latency, and the products from the GNSS Receiver for Atmospheric Sounding (GRAS) Support Network (GSN) with different latencies ranging from 10 to 90 min (Montenbruck et al. 2013). Using the IGS ultra-rapid products, the orbital accuracy of the GRACE and TerraSAR-X satellites has also reached dm-level (Montenbruck et al. 2005; Wermuth et al. 2012). In addition to the Internet-linked real-time GNSS products, the precise orbits and clocks can also be obtained directly through the geostationary earth orbit (GEO) link from commercial services (Javier et al. 2017). As tested in a simulation study for the onboard LEO POD, a promising 3D accuracy of sub-dm level can be achieved using the Fugro G4 service (Hauschild et al. 2016).

In recent years, in addition to the commercial services mentioned above, high-precision real-time multi-constellation GNSS orbits and clocks are broadcast free-of-charge directly from navigation satellites or GEO satellite of the Satellite-Based Augmentation System (SBAS). Examples are the Multi-GNSS Advanced Demonstration of Orbit and Clock Analysis (MADOCA) Precise Point Positioning (PPP) service of the Japanese Quasi-Zenith Satellite System (QZSS), and the new generation of the Australian/New-Zealand (AU/NZ) SBAS-aided PPP service. The MADOCA service, operated by the Japan Aerospace Research and Development Agency (JAXA), provides the precise orbit and clock corrections for GPS, GLONASS, and QZSS, through an Internet link and from the QZSS satellites via the L6E signal (GPAS 2017). Using MADOCA precise corrections, the 3D accuracy of the PPP results is shown to be at a dm-level after convergence for ground receivers (Zhang et al. 2019). For SBAS-aided PPP service, precise corrections are broadcast by the GEO satellite Inmarsat-4F1 within the new generation of AU/NZ SBAS testbed. This provides PPP service via L1 (for GPS L1/L5 signals) and L5 (for GPS L1/L5 and Galileo E1/E5a signals) (Barrios et al. 2018). Note that the initial phase of SBAS-aided PPP service has supported the GPS L1/L2 signals instead of those on L1/L5 to

enable a good measurement geometry and simulate the conditions when more satellites broadcast L5 signals are available. For SBAS-aided L5 PPP service, e.g., tests have also demonstrated a dm-level 3D accuracy for static stations in the open-sky situations (Sobreira et al. 2018), and at decimeters for road transport in suburban environments (El-Mowafy et al. 2020). Although both products (MADOCA and SBAS) have currently regional service over the Asia-Pacific region, in this research, we investigate their potential benefits to the LEO POD, expecting that similar services can be provided by more regional/global navigation satellite systems or SBASs in the future, and global coverage can be reached.

For the first time in this study, POD results are assessed using MADOCA L6E PPP corrections and SBAS-aided L5 PPP corrections that are received through free satellite links. Making use of the real data of two typical LEO satellites from GRACE Follow-On (Flechtner et al. 2014) and Sentinel-3 mission (ESA 2012), the POD is performed in both the reduced-dynamic and the kinematic modes, and applying precise GNSS orbits and clocks of these two services. The results are compared with those achieved using IGS final products and other Internet-linked real-time services, e.g., IGS RTS products, IGS ultra-rapid products, and National Centre for Space Studies (CNES) products (Laurichesse et al. 2013). For the reduced-dynamic mode, the accuracy of LEO satellite velocities using different products, computed from the difference between them and the velocities provided in the reference products, are also analyzed, including analysis for small satellites that may not be able to track the GNSS signals continuously due to their power constraints, such as CubeSats (Wang et al. 2020). The duty cycle, i.e., collecting data within a pre-defined percentage of time due to the power constraints of small satellites that necessities rotating access to power among different sensors, is tested down to 40%, and corresponding influences on the orbital accuracy are assessed.

We first assess the precise orbits and clocks of MADOCA L6E PPP service and SBAS-aided L5 PPP service by comparing them with IGS/CODE final products as reference. The LEO POD processing strategy is then briefly explained for both the kinematic and dynamic modes, followed by a comprehensive analysis of the POD results using different products, for the reduced-dynamic and the kinematic modes and applying different duty cycles. The study is concluded with an outlook for the near future.

Analysis of the precise orbits and clocks used for POD

In different analysis centers, data collected from a network of Continuously Operating Reference Stations

(CORS) are processed using different observation models to estimate parameters such as station coordinates and clocks, tropospheric delays, satellite orbits and clocks, ambiguities, and inter-system biases (Weiss et al. 2017). For the products considered in our study, MADOCA L6E PPP products are computed based on multi-GNSS observations of a global network (JAXA 2020), uploaded to the QZSS satellites, and broadcast through L6E signal to users. The network used to estimate the precise orbits and clocks for AU/NZ SBAS consists of stations from the Australian regional GNSS network, the south pacific GNSS network, the Land Information New Zealand (LINZ) PositioNZ network, and the IGS network. GNSS satellite orbit and clock corrections are estimated at Uralla station in New South Wales, Australia, and transferred to the Inmarsat-4F1 GEO satellite through the uplink system (Barrios et al. 2018).

In the following sub-sections, the accuracy of orbit and clock products of MADOCA L6E PPP service and SBAS-aided L5 PPP service is analyzed and compared with IGS/CODE final products (IGS final 2020), considered as a reference, since IGS final products are known to be among the most accurate available products.

Orbit comparison

The IGS orbits are weighted sums of the reduced-dynamic orbits estimated by different IGS analysis centers and contain the Centre of Mass (CoM) positions of GNSS satellites in the Earth-Centre Earth-Fixed (ECEF) frame, i.e., the IGS14 during our test period in August 2018. The MADOCA orbits also refer to the CoM. However, the orbits of SBAS-aided PPP service are computed with respect to the antenna phase center (APC). To have a consistent comparison, the SBAS orbits are corrected in the inertial system with the offset between the APC and the CoM as follows:

$$r_{\mathrm{I}}^{\mathrm{CoM}} = r_{\mathrm{I}} - x_{\mathrm{SRF}} e_{\mathrm{x}} - y_{\mathrm{SRF}} e_{\mathrm{y}} - z_{\mathrm{SRF}} e_{\mathrm{z}} \tag{1}$$

where $r_{\mathrm{I}}^{\mathrm{CoM}}$ and r_{I} denote the orbital position vectors in the inertial system referred to the CoM and the APC, respectively. The vector $(x_{\mathrm{SRF}}, y_{\mathrm{SRF}}, x_{\mathrm{SRF}})^T$ is the vector from the CoM to the APC expressed in the satellite reference frame (SRF), which is transformed into the inertial system using the unit vectors e_{x}, e_{y} and e_{z} with (Subirana et al. 2013):

$$e_z = -\frac{r_I}{\|r_I\|},\ e_y = e_z \times e_s,\ e_x = e_y \times e_z \tag{2}$$

$$e_s = \frac{r_{sun} - r_I^{CoM}}{\|r_{sun} - r_I^{CoM}\|} \approx \frac{r_{sun}}{\|r_{sun}\|} \tag{3}$$

where r_{sun} is the position of the sun in the inertial frame derived from Jet Propulsion Laboratory Development Ephemeris (JPL DE405) (Montenbruck and Gill 2000), and $\| . \|$ denotes the norm of the vector. The correction is performed with the help of the Bernese GNSS Software Version 5.2 (Dach et al. 2015) having the approximation given in (3).

The corrected orbits of the MADOCA L6E PPP service and SBAS-aided L5 PPP services, after transforming the latter to the CoM, are compared with IGS orbits for seven days from August 14-20, 2018, as a suitable representative period. The sampling interval of the orbit comparison is 30 s. The root mean square error (RMSE) for all available GPS satellites are shown in Figure 1 in the radial, along-track, and cross-track directions. Figure 1 shows that the RMSE values are mostly at a few cm, and the orbital accuracy in the radial direction is better than in the other two directions, mostly below 5 cm for both products. Also, it is visible that MADOCA orbits generally have a 3D RMSE below or around 5 cm. This orbital accuracy of MADOCA products is consistent with those reported in (Zhang et al. 2019). The jump of the red dots on the first test day is caused by abnormal behaviors of satellite G26 orbits in MADOCA products. Large clock jumps are also visible for the same satellite on the same day, which will be shown later.

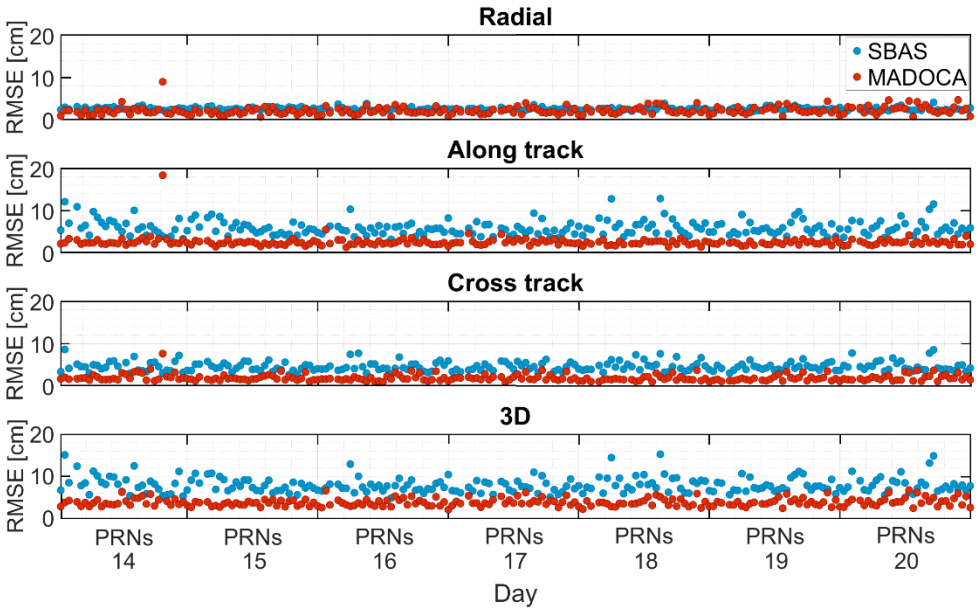

Fig. 1 RMSE of the orbits in MADOCA L6E PPP service (red) and SBAS-aided L5 PPP service (blue) with respect to IGS final orbits in the radial (top), along-track (2nd row), cross-track (3rd row) directions, and the 3D RMS (bottom) for August 14-20, 2018. The area of each day is divided into 31 sections, representing 31 PRNs. Each dot represents the result of one GPS satellite on the corresponding day.

The average orbital RMSE is given in Table 1 over the seven test days. It can be observed that MADOCA L6E and SBAS-aided L5 PPP services have worse orbital accuracy in the along-track direction, i.e., in the direction of the satellite movement than in the other two directions. MADOCA products have shown good orbital consistency with IGS final orbits, i.e., with a 3D RMSE below 4 cm on average.

Table 1 Average orbital RMSE of MADOCA L6E and SBAS-aided L5 PPP services from August 14-20, 2018.

Product	Radial [cm]	Along-track [cm]	Cross-track [cm]	3D [cm]
MADOCA L6E PPP	2.1	2.5	1.8	3.8

SBAS-aided L5 PPP	2.5	5.9	4.5	7.9

Clock comparison

To remove the impact of different time references and enable the clock comparison, we first difference the satellite clocks of MADOCA L6E and SBAS-aided L5 PPP products with IGS final clocks and then subtract the mean clock differences for all available satellites (Yao et al. 2017). The residual Δdt_i^s is expressed as follows:

$$\Delta dt_i^s = dt_{i,\mathrm{IGS}}^s - dt_{i,X}^s - \sum_{n=1}^{n_s} \frac{dt_{i,\mathrm{IGS}}^n - dt_{i,X}^n}{n_s} \quad (4)$$

where $dt_{i,\mathrm{IGS}}^s$ and $dt_{i,X}^s$ denote the clock offsets for satellite s at epoch i from IGS final products and MADOCA or SBAS-aided PPP products (denoted as X), respectively. The number of satellites at epoch i is indicated by n_s . As the constant biases in Δdt_i^s do not significantly influence ambiguity-float processing results, the daily standard deviations (STDs) of Δdt_i^s in ns, shown in Figure 2 for each satellite and each test day, are used for the assessment. The sampling interval of the clock comparison is 30 s. From Figure 2, it can be observed that STD values for MADOCA clocks (red) are generally less than 0.15 ns, and the STDs of SBAS-aided L5 PPP service (blue) are also mostly within 0.2 ns. The 7-days average STD amount to about 0.08 and 0.16 ns, respectively, for MADOCA L6E and SBAS-aided L5 PPP services. Similar to the orbital products, a jump in the red dot on the first day is visible for the G26 clocks.

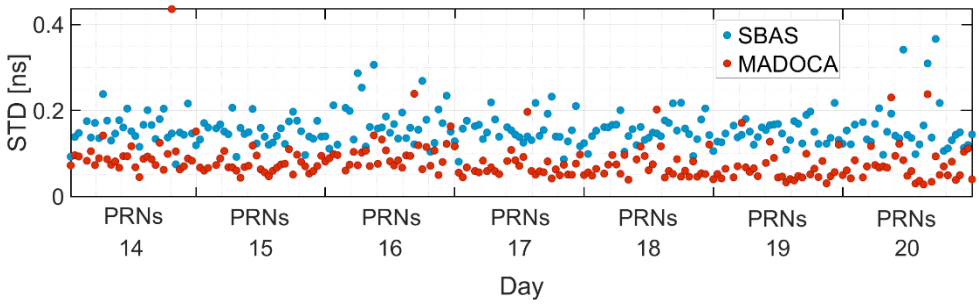

Fig. 2 Standard deviations of the satellite clock residuals from MADOCA L6E PPP service (red) and SBAS-aided L5 PPP service (blue) from August 14-20, 2018. The clocks are compared with IGS final satellite clocks. The area of each day is divided into 31 sections, representing 31 PRNs. Each dot represents the result of

one GPS satellite on the corresponding day.

The short-term stability of the GNSS clocks is essential for high-rate applications such as real-time PPP and radio occultation (Hauschild et al. 2013). To analyze stability of MADOCA and SBAS-aided PPP clocks, we compute their modified Allan deviation (MDEV) (Griggs et al. 2015) and compare with that of CODE final clocks. The results are illustrated in Figure 3 and Table 2. Note that the outlier G26 on August 14, 2020, (see Figure 2) was not used for the calculations. For GPS Block IIF satellites equipped with high-quality rubidium clocks, it can be observed that the short-term stabilities of MADOCA and SBAS-aided PPP clocks are slightly worse than CODE final clocks. However, for MADOCA clocks, a MDEV of about 3×10^{-12}, 1×10^{-12} and 5×10^{-13} can still be reached at an averaging time of 5 s, 30 s and 180 s, respectively.

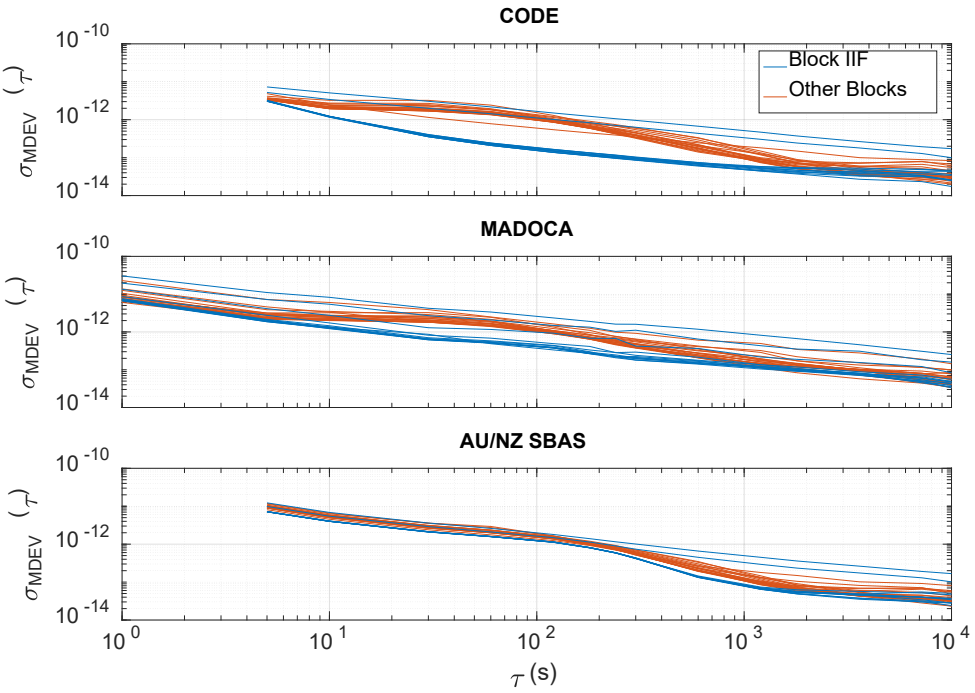

Fig. 3 Modified Allan deviation (σ_{MDEV}) of all GPS clocks from CODE final products (top), MADOCA L6E PPP service (middle), and SBAS-aided L5 PPP service (bottom) from August 14-20, 2018.

Table 2 Mean MDEV of the CODE, MADOCA, and SBAS-aided PPP (L5) clocks for all Block-IIF satellites with

different averaging time. Clocks from August 14-20, 2018, were used in the calculations.

	Mean MDEV ($\times 10^{-12}$)					
Averaging time (s)	**5**	**10**	**30**	**60**	**120**	**180**
CODE	3.67	1.71	0.73	0.48	0.33	0.27
MADOCA	3.41	2.38	1.20	0.95	0.69	0.54
SBAS	7.88	4.41	2.32	1.72	1.22	0.89

The quality difference between MADOCA L6E and SBAS-aided L5 products can be attributed to from the following:

- The network density and distribution used for the two products are different. As shown in Figure 4, MADOCA uses a network of about 90 stations (JAXA 2020), while the network used in the AU/NZ SBAS contains about 60 stations (Barrios et al. 2018). A better global distribution of the network can be observed for MADOCA.
- The constellations used in network processing are different. MADOCA uses observations of GPS, GLONASS, Galileo, BDS, and QZSS (JAXA 2020), while SBAS-aided L5 products are generated using GPS and Galileo signals (personal communication).
- The models used in the network processing are different. For example, MADOCA uses the empirical DBY solar radiation pressure (SRP) model and updates 12 coefficients regularly (Takasu et al. 2015), while AU/NZ SBAS estimates 5 empirical SRP coefficients in the real-time filter (Tobías et al. 2014).
- The update interval of the real-time filter is 1 s for MADOCA, while for AU/NZ SBAS it amounts to 2 s (personal communication).
- The SBAS-aided PPP corrections are codified to the AU/NZ SBAS GEO link's spare bits, which has a limited bandwidth. Compared to using SBAS-aided PPP corrections in the radio technical commission for maritime services (RTCM) format, obvious degradations were reported in PPP results (Rubinov et al. 2019). A different GEO message format is considered to be defined to eliminate this constraint

(personal communication).

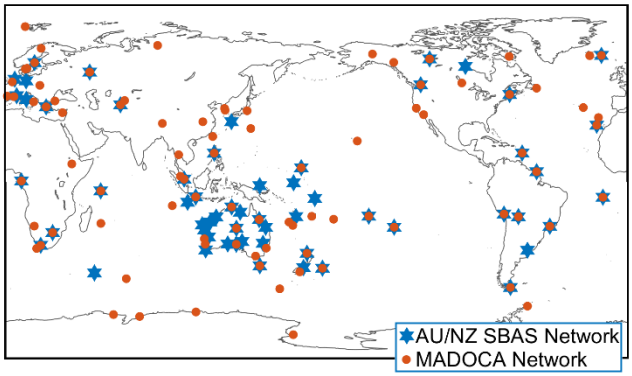

Fig. 4 Network distribution of MADOCA (red), and AU/NZ SBAS services (blue).

Processing strategy

In this study, using Bernese GNSS Software Version 5.2 (Dach et al. 2015), the orbits of LEO satellites are post-processed based on the batch least-squares estimation in both the reduced-dynamic and the kinematic modes. The reduced-dynamic orbit determination is based on solving the following satellite equation of motion as a second-order differential equation by using numerical integration methods:

$$a = -GM\frac{r}{\|r\|^3} + a_{\mathrm{p}} \tag{5}$$

where a is the total acceleration vector, GM is the gravitational constant, and r indicates the satellite position vector. The term a_{p} represents the acceleration vector caused by all other perturbations, which is a function of the satellite positions, velocities, time, and the estimable dynamic parameters, including the constant and periodic dynamic parameters and stochastic velocity changes or constant accelerations in short time intervals (Beutler et al. 2003; Dach et al. 2015). A summary of this procedure is depicted in Figure 5 with the processing details given in Table 3. The POD procedure starts by generating the code-based kinematic positions, which are later combined with the dynamic models to produce an initial coarse orbit. Using GNSS phase observations, this initial orbit is improved during an iterative scheme along with the phase-screening step. In addition to the receiver clock offset and ambiguity terms under the ionosphere-free (IF) combination, 6 Keplerian elements at the initial state are estimated together with additional

dynamic parameters to compensate for model deficiencies of the existing dynamic models used in the processing. This includes 3 constant and 6 periodic dynamic parameters, and stochastic velocity changes within pre-defined intervals, e.g., every 15 min in this study. These estimable parameters are obtained with the least-squares adjustment using GPS observations, and the design matrix is constructed with the help of the partial derivatives of the orbital positions with respect to Kepler elements at the initial condition, the constant/periodic dynamic parameters and stochastic parameters based on the following variational equations (Montenbruck and Gill 2000):

$$\frac{\mathrm{d}}{\mathrm{d}t}\left(\tilde{\Phi},\tilde{S}\right)=\begin{pmatrix}0_{3\times3} & I_{3\times3}\\ \partial_r a & \partial_v a\end{pmatrix}_{6\times6}\left(\tilde{\Phi},\tilde{S}\right)+\begin{pmatrix}0_{3\times6} & 0_{3\times n_p}\\ 0_{3\times6} & \partial_p a\end{pmatrix}_{6\times(6+n_{\mathrm{p}})} \tag{6}$$

where $\tilde{\Phi}=\partial_{r_0,v_0}(r_t^T,v_t^T)^T$ contains partial derivatives of the LEO position and velocity at time t with respect to the initial state vector and $\tilde{S}=\partial_p(r_t^T,v_t^T)^T$ comprises the corresponding partial derivatives with respect to the dynamic parameters p. The number of the dynamic parameters is denoted by n_{p}. Note that the partial derivatives with respect to the stochastic parameters can be obtained by forming linear combinations of those with respect to the osculating elements (Dach et al. 2015). With Keplerian elements at the initial condition and all dynamic parameters estimated, a phase-based reduced-dynamic orbit is produced with the numerical integration of (5). In the end, the reduced-dynamic orbit is further improved by estimating stochastic accelerations within shorter time intervals, e.g., every 6 min.

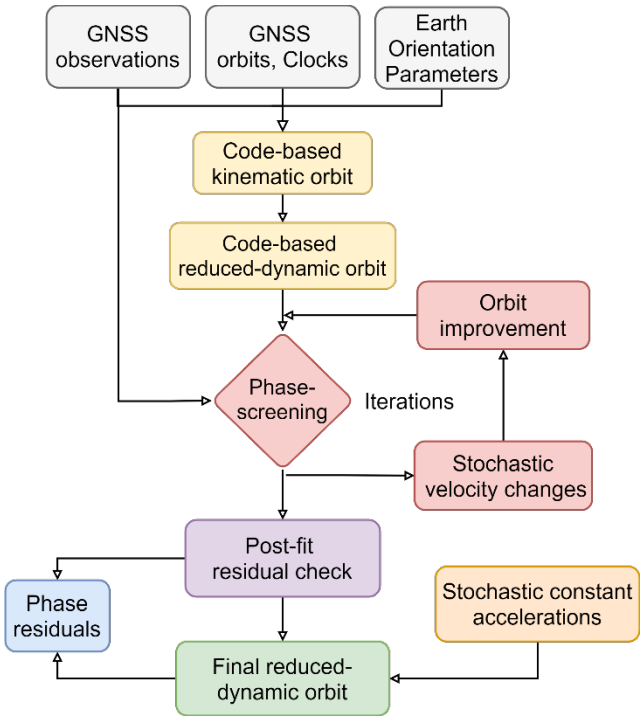

Fig. 5 Flowchart of the reduced-dynamic POD.

Table 3 LEO POD processing models and parameters. EGM is the acronym of the Earth Gravity Model, and IERS stands for the International Earth Rotation and Reference Systems Service.

Item	**Description**
Gravity field	EGM 2008 (120x120) (Pavlis et al. 2008)
Solid earth / Ocean tide	IERS 2010 (Petit and Luzum 2010) / FES2004 (50x50) (Lyard et al. 2006)
Sun, Moon, and other planet ephemerides	DE405 (Standish 1998)
Relativity	IERS 2010
Observation sampling interval	30 s
Observation combination	GPS dual-frequency IF combination
Code and phase standard deviations	0.1 m, 1 mm (Zenith, L1)

Elevation cut-off angle	5 degrees

The kinematic orbits are also estimated based on the dual-frequency GNSS observations using PPP method in addition to the reduced-dynamic orbits. The receiver clock offset and 3D orbital positions are estimated at each epoch independently together with the IF ambiguity terms. In this study, the reduced-dynamic and the kinematic LEO orbits are computed and compared using different real-time products from MADOCA L6E service, SBAS-aided L5 PPP service, and several other Internet-provided real-time services. Details are given in the next section.

Test results

This section presents the final orbits of two satellites from typical LEO missions, i.e., Sentinel-3B satellite from the Sentinel-3 mission and satellite GRACE-FO 1 from the GRACE Follow-On mission, are evaluated as representative examples of LEO satellites for seven days from August 14-20, 2018. Using the precise satellite clocks and orbits delivered by MADOCA PPP L6E service and SBAS-aided L5 PPP service, the LEO orbits are computed in both the reduced-dynamic and the kinematic modes. They are compared with the reference orbits provided by the European Space Agency (ESA) for Sentinel-3B (Fernández 2019) and the JPL for GRACE-FO 1 (Wen et al. 2019).

For comparison, in addition to GPS products from SBAS-aided L5 PPP service and MADOCA PPP L6E service, other precise real-time orbit and clock products were also used for generating the POD solutions. This includes the products from CNES (Laurichesse et al. 2013), the ultra-rapid products from IGS (IGS ultra-rapid 2020), and the products from IGS RTS (IGS RTS 2020). These, however, need ground uplink to LEO satellites, unlike MADOCA and SBAS-aided PPP products, which can be received from higher satellites, thus, facilitating real-time onboard computation. Furthermore, IGS final products, which have a latency of 12 to 18 days, were also utilized for the LEO orbit processing for comparison. Table 4 summarizes the information of different GPS products used to process daily arcs (i.e., processing period). Note that 18 h observed part and 6 h predicted part of IGS ultra-rapid products were used for processing the daily arcs. As an example, for arcs ending at 24:00 in GPS time (GPST), the last available ultra-rapid products are provided at 21:00, which contain 18 h observed part (from 00:00 to 18:00) and 6 h predicted part (from 18:00 to 24:00). It can

be used in such a case.

Table 4 Details of different GPS products used for the processing. Note that the sampling intervals of different real-time products are given based on the real-time orbit and clock files provided by the servers of the corresponding analysis centers, and for SBAS-aided L5 PPP service, provided by the GMV team

Products	**Indicator**	**Transfer**	**Sampling interval [s]**		**Source**
			Orbits	Clocks	
MADOCA L6E PPP	MDC	Internet/QZSS	30	30	JAXA
SBAS-aided L5 PPP	SBS	Internet/GEO	5	5	GMV
IGS final	IGS	Internet	900	30	IGS
CNES real-time	CNE	Internet	300	5	CNES
IGS RTS	IGC	Internet	30	30	IGS
IGS ultra-rapid	IGP	Internet	900	900	IGS

To deal with the power constraints of small satellites (Lantto and Gross 2018), e.g., CubeSats, for the reduced-dynamic orbits, duty cycling, i.e., collecting data in a pre-defined portion of time, is enabled for the testing with the duty cycle varying from 100% to 40%. This implies possible intermittent tracking of GPS signals, and in our tests, for a duty cycle of $D\%$, only the first $D\%$ of the data in each hour are used for the processing. The ambiguities are newly set up after each power-off period.

In the next two sub-sections, the orbital positions using different GPS products are assessed in radial, along-track, and cross-track directions with respect to the corresponding reference orbits (from ESA and JPL), as mentioned before.

Reduced-dynamic orbits

Using MADOCA L6E PPP products and SBAS-aided L5 PPP products, the orbital errors of GRACE FO-1 are illustrated in Figure 6 in the radial, along-track, and cross-track directions for the day August 15, 2018, as a representative example. The duty cycle varies from 100% to 40%. From Figure 6, it can be observed that the orbital differences generally range from sub-dm to dm-level. The errors in the along-track direction are shown to be larger than in the other two directions. The average RMSE in the three directions are given for both test satellites and the seven test days in Table 5. Note that the average RMSE is computed based on the daily RMSE, which used the POD results from the beginning of the first power-on period to the end of the last power-on period in each day. The radial RMSE values are in the range of 1-3 cm even for a duty cycle of 40%, and below 2 cm when using MADOCA products. For example, the latter case fulfills the requirement of 1-2 cm radial accuracy for the altimetry missions (Montenbruck 2017). Making use of both products, 3D RMSE at several centimeters can be achieved for post-processed reduced-dynamic orbits even at a duty cycle of 40%, which satisfies the requirement of the near-real-time POD with sub-dm accuracy that is suitable, for example, for InSAR missions (Montenbruck 2017).

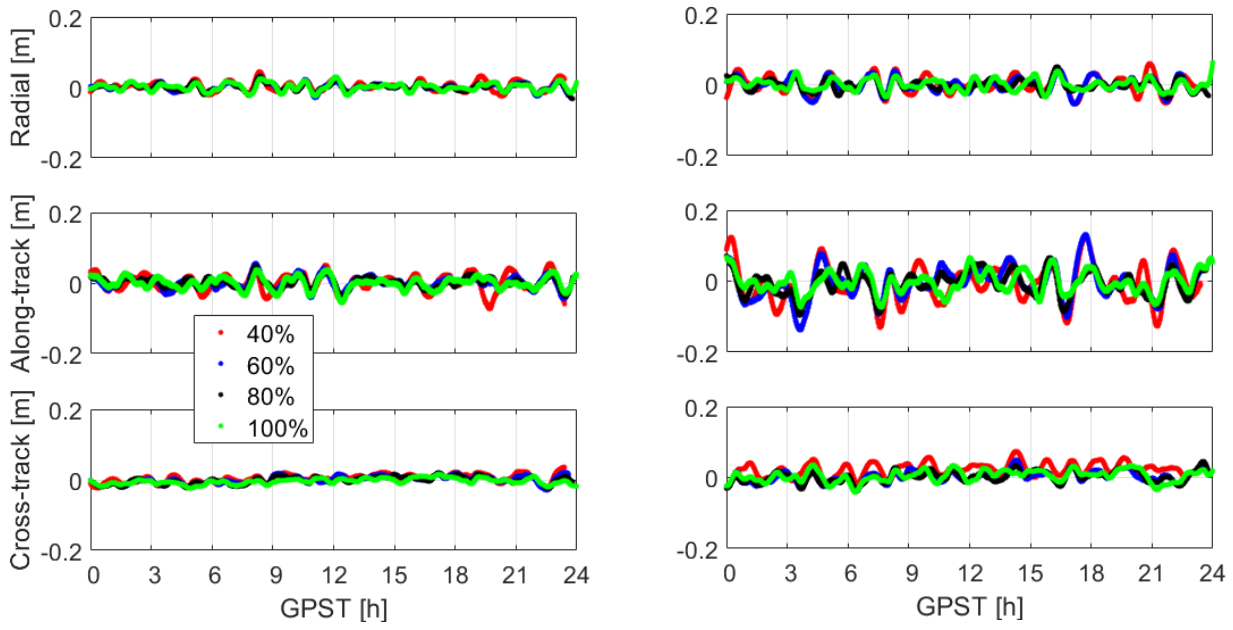

Fig. 6 Orbital differences between the reduced-dynamic orbits and the reference orbits applying (left) MADOCA L6E PPP products and (right) SBAS-aided L5 PPP products. The data of GRACE-FO 1 on August 15, 2018, were used for the plot.

Table 5 Average RMSE of the reduced-dynamic orbits from August 14-20, 2018, using MADOCA L6E PPP products and SBAS-aided L5 PPP products. The results for the satellites GRACE-FO 1 and Sentinel-3B are separated by "/", respectively

Duty cycle	Radial [m]	Along-track [m]	Cross-track [m]	3D [m]
MADOCA L6E PPP products				
100%	0.011/0.016	0.018/0.027	0.009/0.020	0.023/0.037
80%	0.009/0.015	0.016/0.026	0.010/0.021	0.021/0.036
60%	0.010/0.016	0.019/0.029	0.012/0.024	0.025/0.041
40%	0.011/0.019	0.023/0.037	0.014/0.031	0.029/0.052
SBAS-aided L5 PPP products				
100%	0.019/0.023	0.037/0.046	0.019/0.034	0.046/0.062
80%	0.018/0.023	0.036/0.046	0.024/0.036	0.047/0.063
60%	0.020/0.024	0.042/0.051	0.027/0.044	0.054/0.071
40%	0.024/0.028	0.055/0.062	0.037/0.043	0.070/0.080

Using the IGS final and other real-time products as listed in Table 4, the average 3D RMSE over the seven days of testing are illustrated in Figure 7 applying different duty cycles. It can be observed that the 3D RMSE generally increases with the decreasing of duty cycles. The line segment in each bar indicates the range of the daily RMSE over the test period, and large ranges are mostly observed at the low duty cycle of 40% (red bars), which indicates a relatively large variation of the accuracy from day to day. The results using SBAS-aided L5 PPP products are slightly worse than those computed using CNES real-time products and IGS RTS products, but better than those using IGS ultra-rapid products. The orbital results generated using MADOCA L6E PPP products have shown to be the best with the smallest RMSE among all tested real-time

products.

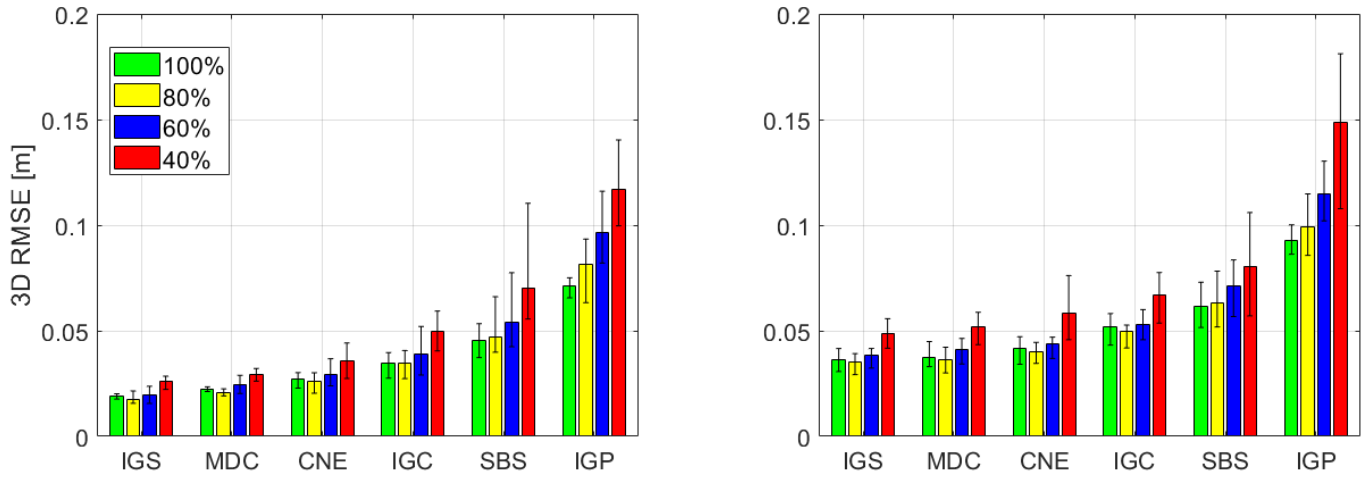

Fig. 7 Average 3D RMSE of the reduced-dynamic orbits applying different duty cycling (shown as the colored percentage in the legend) for (left) GRACE-FO 1 and (right) Sentinel-3B using different GPS products from August 14-20, 2018. The line segments inside each bar illustrate the minimum and maximum daily 3D RMSE over the test period. The abbreviations in the x-axis are given in Table 4.

With a duty cycle of 100%, using the 3D orbital errors for the test period from August 14-20, 2018, the maximum errors within a certain percentage of all 3D orbital errors are illustrated in Figure 8. Figure 8 shows that for both test satellites, 95% of the 3D orbital errors are within or around 1 dm using MADOCA L6E PPP products (black) and SBAS-aided L5 PPP products (cyan). Even with the duty cycle reduced to 40%, 95% of the 3D orbital errors using products of these two services are still within 0.14 m.

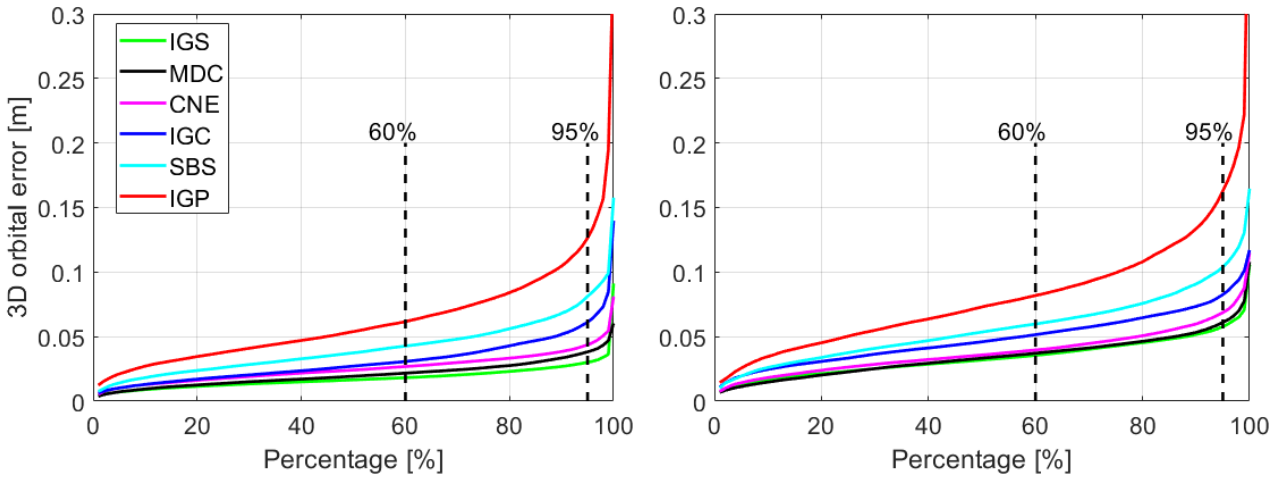

Fig. 8 Maximum 3D errors of the reduced-dynamic orbits within a certain percentage of all 3D orbital errors from August 14-20, 2018, after using different providers of GNSS observation corrections for (left) GRACE-FO1 and (right) Sentinel-3B. The duty cycle is set to 100%

In addition to the satellite positional errors, the satellite velocity errors are also computed for both test satellites using different GPS products in the along-track direction, as the accuracy of the along-track velocity needs to be better than 0.05 to 0.2 mm/s for missions such as GNSS radio occultation (Montenbruck 2017). As shown in Figure 9, the along-track velocities computed using MADOCA L6E and SBAS-aided L5 PPP products have comparable accuracy to those generated using CNES and IGS RTS products, i.e., smaller than 0.05 mm/s on average for all the investigated duty cycles from 40% to 100%. In the cross-track and the radial directions, the average velocity RMSE using these two products (MADOCA and SBAS) are also at a similar level, i.e., within 0.05 mm/s. The velocity RMSE at the radial direction is found to be larger than those in the other two directions. It is noted that in addition to the orbital and velocity accuracy, based on the method used for radio occultation retrieval, short-term clock stability should also be considered (Hauschild et al. 2013, Griggs et al. 2015). This is not, however, within the scope of this study.

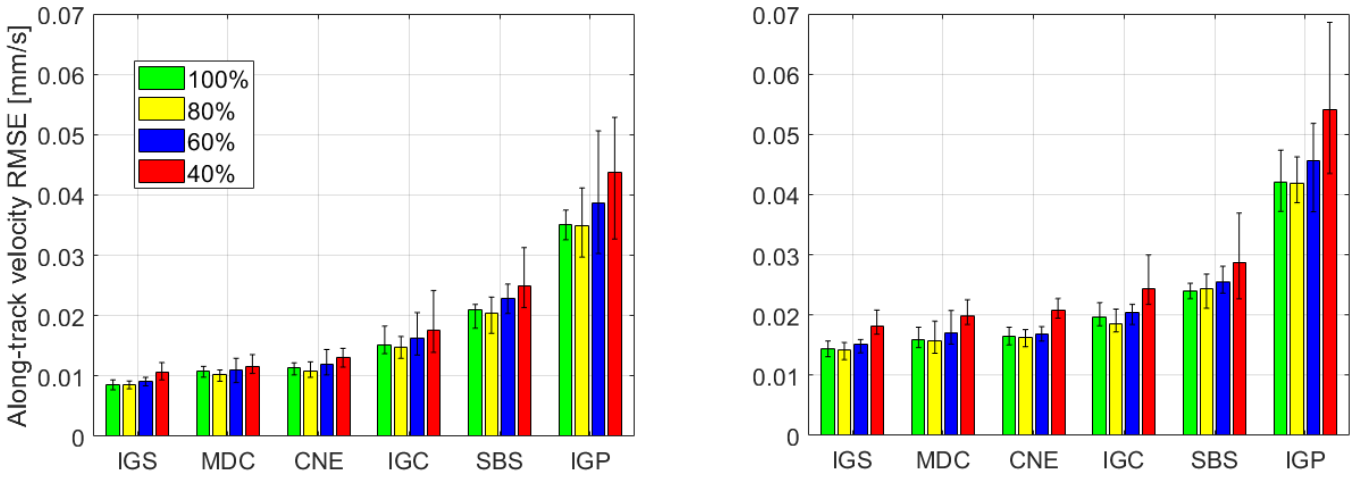

Fig. 9 Average velocity RMSE in the along-track direction for (left) GRACE-FO 1 and (right) Sentinel-3B using different GPS products from August 14-20, 2018. The line segments inside each bar illustrate the minimum and maximum daily velocity RMSE in the along-track direction over the test period. The legend refers to the percentage values for duty cycling

Recall that compared with the other real-time products, MADOCA L6E PPP products and SBAS-aided L5 PPP products can be directly broadcast from QZSS satellites and the geostationary (GEO) SBAS satellite, respectively, and does not necessarily require an internet link. Although the current QZSS constellation and the GEO satellite Inmarsat-4F1 used for AU/NZ SBAS testbed have a regional service over the Asia-Pacific region, the shown results illustrate a bright future when more navigation systems and SBASs could broadcast free precise orbit and clock products to users, so that global coverage of such signals can be achieved. Compared with the orbits computed based on the broadcast ephemeris with a 3D RMSE at sub-meter level (Montenbruck and Ramos-Bosch 2008), the precise satellite orbits and clocks from MADOCA L6E PPP service and SBAS-aided L5 PPP service are able to provide significantly better LEO POD accuracy, even with a low duty cycle. This could also indicate good potential for real-time onboard POD for small LEO satellites, such as CubeSats, in the future.

Kinematic orbits

Compared with the post-processed orbits computation, the onboard real-time POD processing has more

substantial constraints on the computational load, and thus needs to balance between the complexity of the dynamic models used and the POD accuracy. As an extreme case, the kinematic orbits are presented in this sub-section, with the final least-squares adjustment (Figure 5) performed based only on GPS measurements. Here a 100% duty cycle is assumed when processing the kinematic orbits. Note that the accuracy of the kinematic orbits post-processed in this study should be similar to that of the converged orbits processed in real-time, provided that GPS L1 and L2 observations are tracked with 100% duty cycle, and processed with comprehensive dynamic models as described in Section "Processing strategy".

As an example, the kinematic orbits are shown together with the reduced-dynamic orbits in Figure 10 for GRACE-FO 1 on August 15, 2018, applying MODACA L6E PPP products (left panel) and SBAS-aided L5 PPP products (right panel). Without applying dynamic models, the kinematic POD orbital errors (red dots) have shown a larger range. The degradation of the kinematic POD results is especially obvious in the radial direction due to the strong correlation between the LEO receiver clock offset and the radial component of the orbit (Rothacher and Beutler 1998).

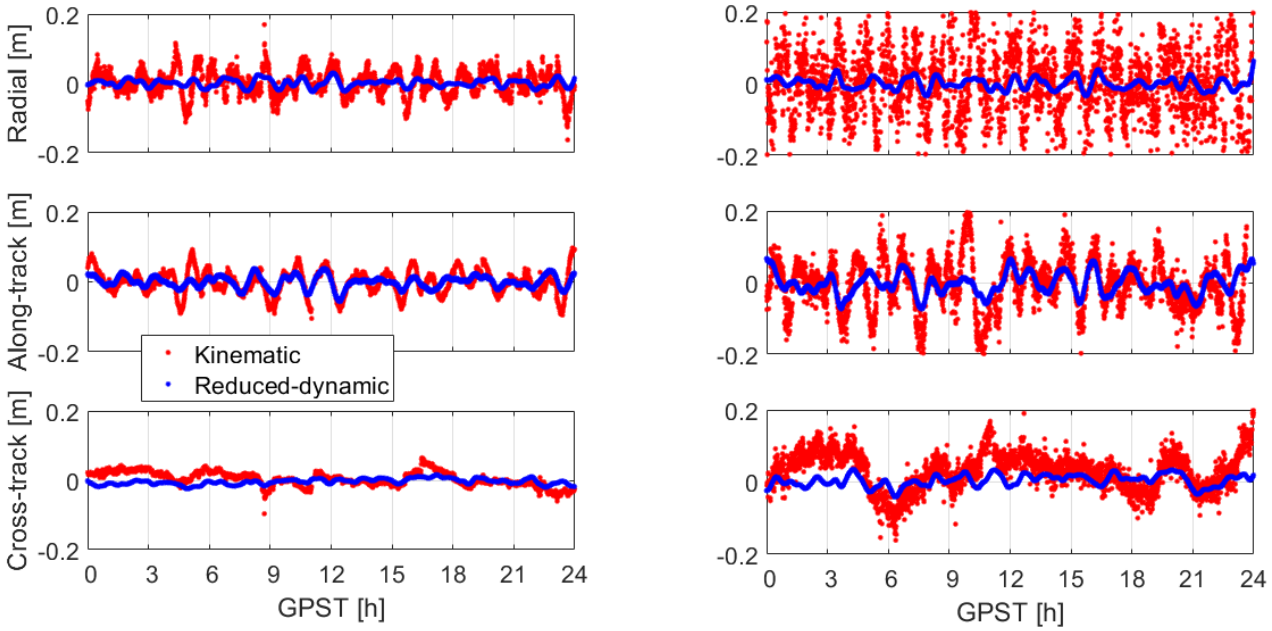

Fig. 10 Kinematic and reduced-dynamic orbits for GRACE FO-1 on August 15, 2018, using (left) MADOCA L6E PPP products and (right) SBAS-aided L5 PPP products

Averaging over all the seven test days, we show the RMSE values in Table 6 for the radial, along-track, and cross-track directions for both GRACE-FO 1 and Sentinel-3B satellites. An outlier detection and exclusion scheme was applied for the kinematic solutions in each direction to screen out large outliers before calculating the RMSE. This process is performed such that the absolute value of the normalized orbital error (assumed normally distributed) in each direction is compared with a threshold K, defined with a significance probability level α arbitrarily taken as 10^{-4}, where:

$$K = Q^{-1}\left(1 - \frac{\alpha}{2}\right) \tag{7}$$

for which Q^{-1} denotes the inverse CDF of a normal distribution. In case that the absolute normalized error is larger than K in any of the three directions, the orbits at the corresponding time point are not used for computing the RMSE. Table 6 shows that the 3D RMSE of the kinematic orbits can generally reach sub-dm to dm-level using MADOCA and SBAS (L5) PPP products among the three directions, the RMSE of the radial orbits is larger than those in the other two directions.

Table 6 Average RMSE of the kinematic orbits from August 14-20, 2018, using MADOCA L6E PPP products and SBAS-aided L5 PPP products. The results for GRACE-FO 1 and Sentinel-3B are separated with "/", respectively.

Product	Radial [m]	Along-track [m]	Cross-track [m]	3D [m]
MADOCA PPP L6E	0.034/0.046	0.032/0.045	0.022/0.043	0.052/0.077
SBAS-aided PPP L5	0.102/0.110	0.081/0.098	0.060/0.079	0.143/0.167

A comparison of the kinematic orbits produced using different precise GPS orbits and clocks is illustrated in Figure 11. Similar to the reduced-dynamic orbits, the results applying SBAS-aided L5 PPP products are slightly worse than those using CNES (CNE) and IGS RTS (IGC) products but are better than those using IGS ultra-rapid (IGP) orbits and clocks. The MADOCA L6E PPP products can produce better

kinematic orbits than all other tested real-time products. A larger RMSE can generally be observed in the radial direction (blue bars) than in the along-track (yellow bars) and the cross-track directions (green bars). In general, it can be observed that the kinematic solutions using MADOCA L6E and SBAS-aided L5 PPP products are at a comparable level to the results applying other real-time precise products, however, without the requirement of an internet link.

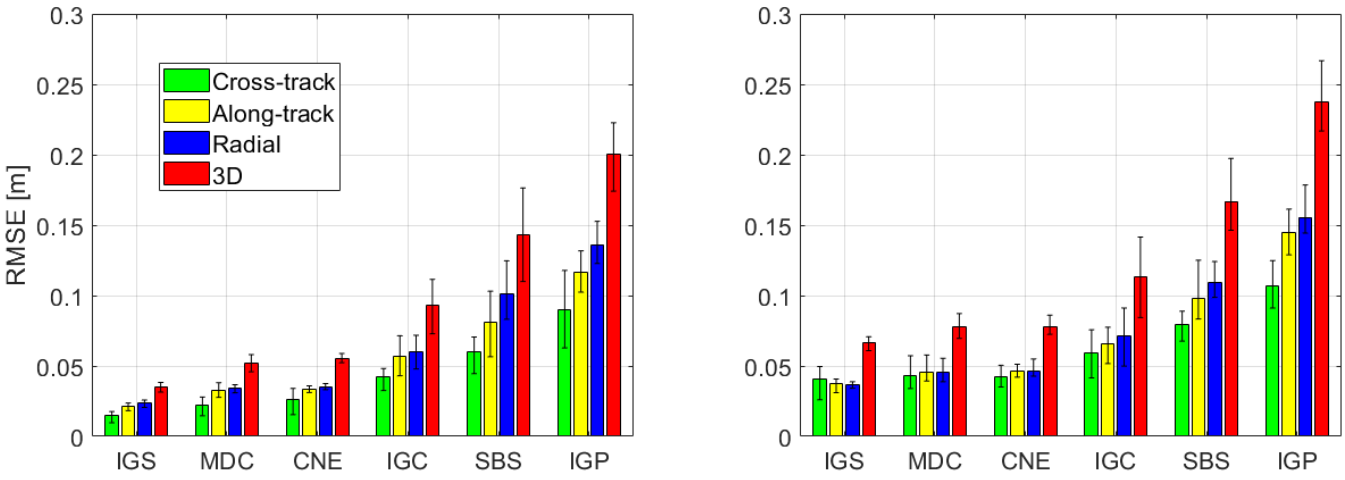

Fig. 11 Average RMSE of the kinematic orbits (for the 3D, cross-track, along-track, and radial directions) for (left) GRACE-FO 1 and (right) Sentinel-3B using different GPS products from August 14-20, 2018. The line segments inside each bar illustrate the minimum and maximum daily RMSE over the test period

Using the 3D errors of the kinematic orbits over the seven test days, including also outliers, the maximum errors within different percentages of all 3D orbital errors are illustrated for the two test satellites in Figure 12. It can be observed that the maximum errors within 60% of all errors are at sub-dm to dm-level using the products from MADOCA (black) and SBAS-aided L5 PPP services (cyan). 95% of the kinematic orbital errors are within or around 1 dm using MADOCA L6E PPP products and are within 3 dm using SBAS-aided PPP L5 products.

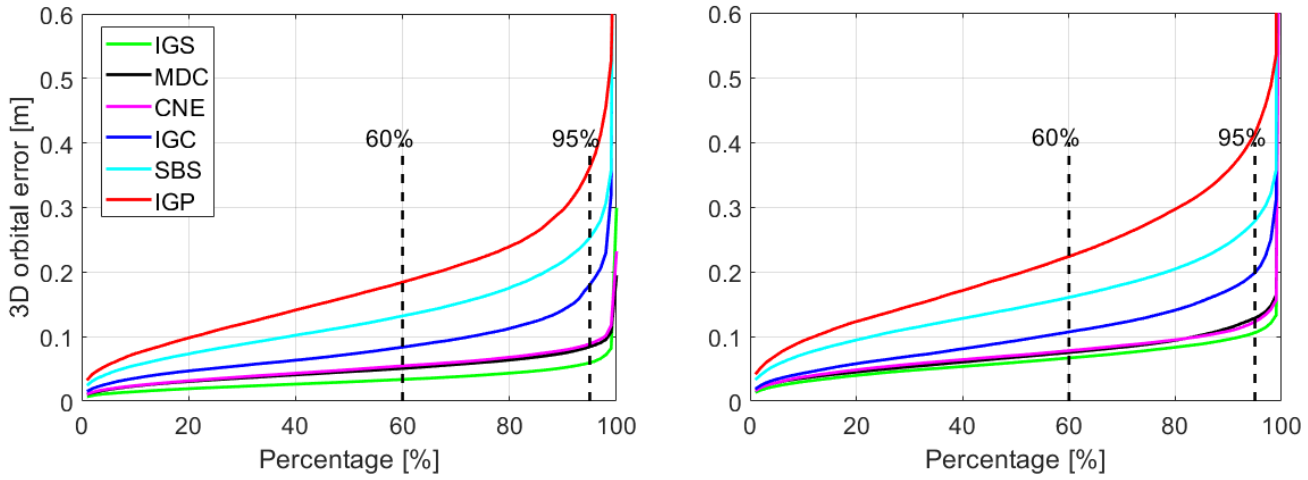

Fig. 12 Maximum 3D errors of the kinematic orbits within a certain percentage of all 3D orbital errors from August 14-20, 2018, using different providers of GPS observation corrections for (left) GRACE-FO 1 and (right) Sentinel-3B satellites. The duty cycle is set to 100%.

Conclusion

Nowadays, different real-time services provide precise GNSS satellite orbits and clock corrections to users, benefiting the POD of spaceborne receivers onboard LEO satellites. While most real-time services on the ground require an Internet link to transmit their products, in recent years, non-commercial services broadcast multi-constellation GNSS orbits and clock corrections directly from navigation satellites or GEO SBAS satellites. The Japanese MADOCA L6E PPP service and AU/NZ SBAS-aided L5 PPP service are two good examples for this purpose.

This study shows that GPS orbit and clock corrections of these two products are of high accuracy. Using these two products, the orbital accuracy of the tested LEO satellites ranges at several centimeters even with a duty cycle down to 40% in the reduced-dynamic mode, which is comparable to those using other high-quality Internet-linked real-time products and fulfills the requirement for applications like InSAR. The results demonstrated that 95% of the reduced-dynamic orbital errors are within or around 1 dm using the two new tested products with a duty cycle of 100%. Among all the three directions, the accuracy of the radial component using MADOCA PPP products is below 2 cm even having a 40% duty cycle, which fulfills the requirement of satellite altimetry. The velocity accuracy is within 0.05 mm/s in the along-track direction,

which is useful for the GNSS radio occultation missions. The 3D orbital accuracy is at sub-dm to dm-level in the kinematic mode using MADOCA and SBAS-aided (L5) PPP products. The orbits computed using MADOCA products have generally shown better accuracy than the results using all other tested real-time products, including those from CNES and IGS RTS. The orbits computed using SBAS-aided L5 PPP products have also over-performed those using IGS ultra-rapid products.

The results shown in this study, on one side, demonstrate the high-quality of MADOCA and SBAS-aided real-time GNSS products, and on the other side, illustrate a bright future for precise onboard LEO POD, which benefits from these high-precision, satellite-linked, and free-of-charge GNSS products instead of using low-accuracy broadcast ephemeris. Furthermore, for small satellites with power constraints, such as CubeSats, good orbital accuracy is shown to be achievable, albeit in the post-processing mode mimicking real-time applications after convergence, using these two products even with a duty cycle down to 40%.

Acknowledgement

We would like to thank the GMV team for providing the GNSS satellite orbits and clocks of the SBAS-aided L5 PPP service. Special thanks are given to Julián Barrios from GMV and Hiroshi Takiguchi from JAXA for discussions of the processing details of the MADOCA and the SBAS-aided PPP products. The work is funded by the Australian Research Council Discovery Project: Tracking Formation-Flying of Nanosatellites Using Inter-Satellite Links (DP 190102444).

Data Availability The MADOCA L6E PPP products were obtained from the JAXA ftp://mgmds01.tksc.jaxa.jp/mdc1/. The IGS final, ultra-rapid, and the RTS products were obtained from the NASA CDDIS https://cddis.nasa.gov/archive/gnss/products/rtpp/. The CNES real-time products were obtained from http://www.ppp-wizard.net/products/REAL_TIME/. The data of GRACE FO-1 were obtained from the NASA JPL https://podaac-tools.jpl.nasa.gov/drive/files/allData/gracefo/L1B/JPL/RL04/ASCII/. The observation data and the reference orbits of the Sentinel-3B were obtained from the ESA via https://scihub.copernicus.eu/gnss/#/home and https://sentinel.esa.int/web/sentinel/missions/sentinel-3/ground-segment/pod/products-requirements, respectively. The SBAS-aided PPP L5 corrections are

available from the corresponding author on reasonable request. The data are processed with the Bernese GNSS software Version 5.2.

References

Barrios J, Caro J, Calle JD, Carbonell E, Pericacho JG, Fernández G, Esteban VM, Fernández MA, Bravo F, Torres B (2018) Update on Australia and New Zealand DFMC SBAS and PPP System Results. In Proc. ION GNSS+ 2018, Institute of Navigation, Miami, Florida, USA, September 24-28, 1038-1067.

Barrios J, Caro J, Calle JD, Carbonell E, Pericacho JG, Fernández G, Esteban VM, Fernández MA, Bravo F, Torres B, Calabrese A (2019) Australia and New Zealand SBAS and PPP Testbed. System on Track. In Proc. ION GNSS+ 2019, Institute of Navigation, Miami, Florida, USA, September 16-20, 876-901.

Beutler G, Schildknecht T, Hugentobler U, Gurtner W (2003) Orbit determination in satellite geodesy. Adv Space Res 31(8):1853-1868. doi:10.1016/S0273-1177(03)00171-6

Dach R, Lutz S, Walser P, Fridez P (2015) Bernese GNSS Software Version 5.2. University of Bern, Bern Open Publishing. doi:10.7892/boris.72297

El-Mowafy A, Cheung N, Rubinov E (2020) First results of using the second generation SBAS in Australian urban and suburban road environments. J Spat Sci 65:99-121. doi:10.1080/14498596.2019.1664943

ESA (2012) SENTINEL-3, ESA's Global Land and Ocean Mission for GMES Operational Services. European Space Agency. https://sentinel.esa.int/documents/247904/351187/S3_SP-1322_3.pdf.

Fernández M (2019) Sentinel-3 Properties for GPS POD, Copernicus Sentinel-1, -2 and -3 Precise Orbit Determination Service (SENTINELSPOD), GMV-GMESPOD-TN-0027, Version 1.7. https://sentinels.copernicus.eu/documents/247904/3372613/Sentinel-3-GPS-POD-Properties.pdf.

Flechtner F, Morton P, Watkins M, Webb F (2014) Status of the GRACE follow-on mission. In: Gravity, geoid and height systems, IAG Symposia, vol 141. Springer, Cham, Switzerland. pp. 117-121. doi: 10.1007/978-3-319-10837-7_15

GPAS- Global Positioning Augmentation Service Corporation (2017) L6E MADOCA Data Format

http://file.gpas.co.jp/L6E_MADOCA_DataFormat_E.pdf.

Griggs E, Kursinski ER, Akos D (2015) Short-term GNSS satellite clock stability. Radio Science, 50(8):813-826. doi:10.1002/2015RS005667

Hadas T, Bosy J (2015) IGS RTS precise orbits and clocks verification and quality degradation over time. GPS Solut. 19:93-105. doi:10.1007/s10291-014-0369-5

Hauschild A, Montenbruck O, Steigenberger P (2013) Short-term analysis of GNSS clocks. GPS Solut. 17:295-307. doi:10.1007/s10291-012-0278-4

Hauschild A, Tegedor J, Montenbruck O, Visser H, Markgraf M (2016) Precise onboard orbit determination for LEO satellites with real-time orbit and clock corrections. In Proc. ION GNSS+ 2016, Institute of Navigation, Portland, Oregon, USA, September 12-16, 3715-3723.

IGS final (2020) International GNSS Service, GNSS Final Combined Orbit Solution Product. Greenbelt, MD, USA: NASA Crustal Dynamics Data Information System (CDDIS). doi:10.5067/gnss/gnss_igsorb_001

IGS RTS (2020) International GNSS Service, Decoded orbit solution (30 second) from IGS real-time product streams. Greenbelt, MD, USA: NASA Crustal Dynamics Data Information System (CDDIS). doi:10.5067/GNSS/gnss_igsrtclk30_001

IGS ultra-rapid (2020) International GNSS Service, GNSS Ultra-Rapid Combined Orbit Solution Product. Greenbelt, MD, USA: NASA Crustal Dynamics Data Information System (CDDIS). doi:10.5067/gnss/gnss_igsuorb_001

Tegedor J, Ørpen O, Melgard T, Łapucha D, Visser H (2017) G4 Multi-constellation Precise Point Positioning Service for High Accuracy Offshore Navigation. International Journal on Marine Navigation and Safety of Sea Transportation, 11(3):425-429. doi:10.12716/1001.11.03.05

JAXA (2020) MADOCA Real-Time Estimate Condition. JAXA. https://ssl.tksc.jaxa.jp/madoca/public/public_message_en.html.

Johnston G, Riddell A, Hausler G (2017) The International GNSS Service. In: Teunissen PJG, Montenbruck O (eds) Springer Handbook of Global Navigation Satellite Systems. Springer, Cham, Switzerland. doi:10.1007/978-3-319-42928-1_33

Lantto S, Gross JN (2018) Precise Orbit Determination Using Duty Cycled GPS Observations. In: 2018 AIAA Modeling and Simulation Technologies Conference, Kissimmee, Florida, USA, January 8-12, 2018. doi: 10.2514/6.2018-1393

Laurichesse D, Cerri L, Berthias JP, Mercier F (2013) Real time precise GPS constellation and clocks estimation by means of a Kalman filter. In Proc. ION GNSS+ 2013, Institute of Navigation, Nashville, TN, USA, September 16-20, 1155-1163.

Lyard F, Lefevre F, Letellier T, Francis O (2006) Modelling the global ocean tides: modern insights from FES2004. Ocean Dynam. 56:394-415. doi:10.1007/s10236-006-0086-x

Montenbruck O (2017) Space Applications. In: Teunissen PJG, Montenbruck O (eds) Springer Handbook of Global Navigation Satellite Systems. Springer International Publishing, Cham, Switzerland. pp 933-964. doi:10.1007/978-3-319-42928-1_32

Montenbruck O, Gill E (2000) Satellite Orbits: Models, Methods and Applications. Springer, Berlin, Heidelberg, Germany. doi:10.1007/978-3-642-58351-3

Montenbruck O, Gill E, Kroes R (2005) Rapid orbit determination of LEO satellites using IGS clock and ephemeris products. GPS Solut. 9:226-235. doi:10.1007/s10291-005-0131-0

Montenbruck O, Hauschild A, Andres Y, von Engeln A, Marquardt C (2013) (Near-) real-time orbit determination for GNSS radio occultation processing. GPS Solut. 17:199-209. doi:10.1007/s10291-012-0271-y

Montenbruck O, Ramos-Bosch P (2008) Precision real-time navigation of LEO satellites using global positioning system measurements. GPS Solut. 12:187-198. doi:10.1007/s10291-007-0080-x

Pavlis N, Kenyon S, Factor J, Holmes S (2008) Earth gravitational model 2008. In: SEG Technical Program Expanded Abstracts 2008. SEG Technical Program Expanded Abstracts. Society of Exploration Geophysicists, pp 761-763. doi:10.1190/1.3063757

Petit G, Luzum B (2010) IERS conventions. (IERS Technical Note; 36) Frankfurt am Main: Verlag des Bundesamts für Kartographie und Geodäsie, 2010. 179 pp., ISBN 3-89888-989-6

Rothacher M, Beutler G (1998) The role of GPS in the study of global change. Phys Chem Earth 23:1029-1040. doi:10.1016/S0079-1946(98)00143-8

Rubinov E, Marshall C, Ng L, Tengku AR (2019) Positioning performance of SBAS and PPP technology from the Australia and New Zealand SBAS test-bed. In Proceedings of the 15th South East Asian Survey Congress (SEASC2019), Darwin, Australia, August 15-18, 1-15. Accessed on December 16, 2020 at https://frontiersi.com.au/wp-content/uploads/2020/11/Rubinov-2019-Results-of-SBAS-Test-bed-SEASC2019.pdf

Sobreira H, Bougard B, Barrios J, Calle JD (2018) SBAS Australian-NZ Test Bed: Exploring New Services. In Proc. ION GNSS+ 2018, Institute of Navigation, Miami, Florida, September 24-28, 2119-2133.

Standish E (1998) JPL planetary and lunar ephemerides, DE405/LE405, JPL IOM 312. F-98_048

Subirana JS, Zornoza JJ, Hernández-Pajares M (2013) GNSS data processing. Volume I: Fundamentals and algorithms. ESA TM-23/1, May 2013. ESA Communications, Noordwijk, the Netherlands.

Švehla D, Rothacher M (2003) Kinematic and reduced-dynamic precise orbit determination of low earth orbiters. Adv Geosci. 1:47-56. doi:10.5194/adgeo-1-47-2003

Takasu T, Miyoshi M, Kaori K, Satoshi K (2015) QZSS-1 Precise Orbit Determination by MADOCA. In: International Symposium on GNSS, Kyoto, Japan, Nov 16-18, 2015.

Tobías G, Calle JD, Navarro P, Rodríguez I, Rodríguez D (2014) magicGNSS'Real-Time POD and PPP Multi-GNSS Service. In Proc. ION GNSS+ 2014, Institute of Navigation, Tampa, Florida, USA, September 8-12, 1046-1055.

Wang K, Allahvirdi-Zadeh A, El-Mowafy A, Gross JN (2020) A Sensitivity Study of POD Using Dual-Frequency GPS for CubeSats Data Limitation and Resources. Remote Sens. 12(13):2107 doi:10.3390/rs12132107

Weiss JP, Steigenberger P, Springer T (2017) Orbit and Clock Product Generation. In: Teunissen PJG, Montenbruck O (eds) Springer Handbook of Global Navigation Satellite Systems. Springer International Publishing, Cham, Switzerland. pp. 983-1010. doi:10.1007/978-3-319-42928-1_34

Wen HY, Kruizinga G, Paik M, Landerer F, Bertiger W, Sakumura C, Bandikova T, Mccullough C (2019) Gravity Recovery and Climate Experiment Follow-On (GRACE-FO). Level-1 Data Product User Handbook vol JPL D-56935 (URS270772).

Wermuth M, Hauschild A, Montenbruck O, Kahle R (2012) TerraSAR-X precise orbit determination with

real-time GPS ephemerides. Adv Space Res. 50:549-559. doi:10.1016/j.asr.2012.03.014

Wu SC, Yunck TP, Thornton CL (1991) Reduced-dynamic technique for precise orbit determination of low earth satellites. J Guid Control Dynam. 14:24-30. doi:10.2514/3.20600

Yao Y, He Y, Yi W, Song W, Cao C, Chen M (2017) Method for evaluating real-time GNSS satellite clock offset products. GPS Solut. 21:1417-1425. doi:10.1007/s10291-017-0619-4

Zhang S, Du S, Li W, Wang G (2019) Evaluation of the GPS precise orbit and clock corrections from MADOCA real-time products. Sensors 19(11), 2580. doi:10.3390/s19112580

Author Biographies

Amir Allahvirdi-Zadeh is a Ph.D. student in the School of Earth and Planetary Sciences, Curtin University. His research interests include precise orbit determination of LEO satellites, especially CubeSats, as well as their applications in space missions.

Kan Wang received her Ph.D. in GNSS advanced modeling from ETH Zurich in 2016 and is a research fellow in the School of Earth and Planetary Sciences, Curtin University. Her research interests include high-precision GNSS positioning, LEO precise orbit determination, SBAS, and integrity monitoring.

Ahmed El-Mowafy obtained his Ph.D. from the University of Calgary, Canada, in 1995 and is the Leader of the GNSS Satellite Positioning and Navigation Group, and Director of Graduate Research, School of Earth and Planetary Sciences, Curtin University, Australia. He has extensive publications in precise positioning and navigation using GNSS, quality control, integrity monitoring and estimation theory.